CHEMISTRY OF MATERIALS

ARTICLE

pubs.acs.org/cm

Phosphates as Lithium-Ion Battery Cathodes: An Evaluation Based on High-Throughput *ab Initio* Calculations

Geoffroy Hautier, Anubhav Jain, Shyue Ping Ong, Byoungwoo Kang, Charles Moore, Robert Doe, and Gerbrand Ceder*

Massachusetts Institute of Technology, Department of Materials Science and Engineering, 77 Massachusetts Avenue, Cambridge, MA 02139

Supporting Information

ABSTRACT: Phosphate materials are being extensively studied as lithium-ion battery electrodes. In this work, we present a high-throughput *ab initio* analysis of phosphates as cathode materials. Capacity, voltage, specific energy, energy density, and thermal stability are evaluated computationally on thousands of compounds. The limits in terms of gravimetric and volumetric capacity inherent to the phosphate chemistry are determined. Voltage ranges for all redox couples in phosphates are provided, and the structural factors influencing the voltages are analyzed. We reinvestigate whether phosphate materials are inherently safe and find that, for the same oxidation state, oxygen release happens thermodynamically at lower temperature for phosphates than for oxides. These findings are used to recommend specific chemistries within the phosphate class and to show the intrinsic limits of certain materials of current interest (e.g., $LiCoPO_4$ and $LiNiPO_4$).

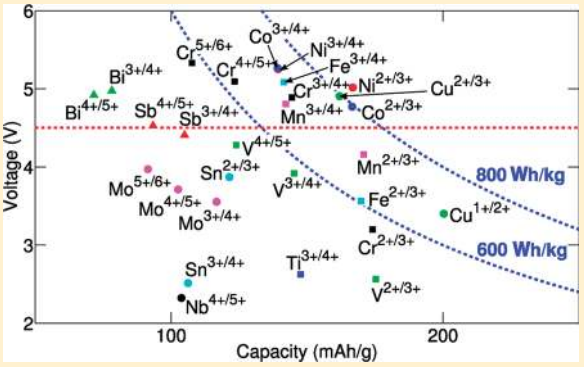

KEYWORDS: Li-ion battery, cathode, phosphates, *ab initio*, DFT, high-throughput, thermal stability, safety

1. INTRODUCTION

The first commercial lithium-ion batteries, appearing in the market in the early 1990s, were based on transition metal oxide cathodes such as layered $LiCoO_2$.[1] In 1997, lithium iron phosphate ($LiFePO_4$) in the olivine structure was demonstrated as a viable cathode material.[2] Since then, the exceptional safety and improvements in rate capabilities of lithium iron phosphate have led to a strong focus from the battery community on polyanionic chemistries and especially on phosphates.[3,4]

Despite the important amount of work on phosphate materials, few phosphates have been precisely characterized and tested electrochemically: $LiMnPO_4$,[5] $LiVOPO_4$,[6] $Li_3Fe_2(PO_4)_3$,[7] $Li_3V_2(PO_4)_3$.[8] The limited size of this data set makes it difficult to understand the trends and limits of phosphates as battery electrodes. Moreover, comparison between experimentally tested materials is sometimes challenging as electrochemical measurement are the result of many different intrinsic and extrinsic materials properties (e.g., rate can be controlled by limitations from the intrinsic materials transport or by electrode fabrication and structure).

Ab initio computations in the density functional theory (DFT) framework have been used for almost 20 years in the battery field to provide insight into the fundamental properties of electrode materials .[9−18] *Ab initio* computations are nowadays accurate enough to understand and even predict many important battery properties (e.g., voltage, stability, safety, and lithium diffusion). The high scalability of computing furthermore offers the possibility to search for new cathode materials using a computational high-throughput approach by computing properties on thousands of potential battery materials. This approach can be used to screen and discover new or overlooked compounds (see for instance Kim et al.[19]) but also to analyze, using a large data set, the limits and factors that control electrochemical properties across an entire chemical class.

In this work, we compute the voltage, capacity (gravimetric and volumetric), specific energy, energy density, stability, and safety of thousands of phosphate compounds using such a computational high-throughput approach. From this large database of calculated properties on phosphates, important conclusions can be made on the limits and opportunities for phosphates as cathode materials.

2. METHODS

2.1. *Ab Initio* High-Throughput Methodology. All *ab initio* computations were performed in the density functional theory (DFT) framework using a generalized gradient approximation (GGA) functional parametrized by Perdew-Burke and Ernzerhof (PBE).[20] The transition metals, Cu, Fe, Cr, Co, Mn, Ni, V, Nb, and Mo, have been

Received: April 2, 2011
Revised: June 19, 2011
Published: July 13, 2011

assigned a U parameter to correct for the self-interaction error present in GGA.[21,22] This U parameter was fitted to experimental binary metal formation energies using the Kubaschewski tables,[23] following the approach of Wang et al.[24] The only exception is the U for Co, set at 5.7 eV, following Zhou et al.[25] We followed Wang et al. and did not use a U parameter on Ti. While hybrid functional, for instance in the Heyd-Scuseria-Ernzerhof (HSE) scheme,[26] can also correct for the self-interaction error,[27] the high-throughput nature of our work favors the use of the less computationally expensive GGA+U framework.

All compounds were run in their ferromagnetic states with a *k*-point density of at least 500/(number of atom in unit cell) *k*-points. The Vienna *ab initio* software package (VASP)[28] was used with the plane-augmented wave (PAW) pseudopotentials provided.[29] The computations are expected to be converged within a few meV/at. More details on the high-throughput *ab initio* methodology can be found in Jain et al.[30]

2.2. Compounds Data Set. Our list of redox active elements and allowed oxidation state consists of Ti (+2 to +4), V (+2 to +5), Cr (+2 to +6), Mn (+2 to +4), Fe (+2 to +4), Co (+2 to +4), Ni (+2 to +4), Cu (+1 to +3), Nb (+3 to +5), Mo (+3 to +6), Sn (+2 to +4), Sb (+3 to +5) and Bi (+3 to +5).

Our set of known compounds was obtained from the 2006 ICSD database.[31] All known compounds containing lithium, phosphorus, oxygen, and a redox active metal were considered.

Duplicate crystal structures were identified and removed using an affine mapping technique. Two structures are considered equivalent if an affine mapping exists transforming one into another within reasonable tolerances.[32] The algorithm used to perform this comparison was based on Hundt et al.[33] This algorithm was also used to assign a crystal structure prototype to any of the generated compounds.

The experimental crystallographic data of some known compounds contain partial occupancies. For those, we used an ordering procedure to enumerate unique supercells using an algorithm proposed by Hart.[34] Among all the enumerated structures, the closest to the structure's stoichiometry, as listed in the ICSD, and lowest in electrostatic energy (according to an Ewald summation on formal valence point charges) was chosen.

In addition to known compounds from the ICSD, we generated "virtual" compounds by substituting ions in known ICSD compounds to form new possible compounds containing lithium, phosphorus, oxygen, and a redox active metal . This substitution process was driven by a data-mined substitution model presented in Hautier et al.[35]

To evaluate stability of the computed compounds, all competing phases known in the ICSD were also computed. For instance, to make the stability study of a Li−M−P−O system possible, we computed the compounds present in the ICSD in all the related binary (i.e., Li−O, M−O, Li−M) and ternary (i.e., Li−M−O, Li−P−O, M−P−O, Li−M−P) systems.[36] In addition, a data-mined ternary oxide structure prediction algorithm has been used to propose any likely new compound candidate in the M−P−O systems.[37] In total, our database contains 4074 computed compounds containing containing lithium, a redox active element, phosphorus. and oxygen.

2.3. Local Environment Assignment. The local environment for a given cation was assigned automatically through a polyhedron matching algorithm. The cation's neighboring oxygen atoms were detected through a Voronoi construction.[38] In a second step, the polyhedron formed by this set of neighbors was compared to a library of perfect local environments (containing environments such as octahedral, square planar, tetrahedral, square pyramidal, trigonal bipyramidal, trigonal prismatic square face monocapped, trigonal, and square antiprismatic). The comparison was performed using the continuous symmetry algorithm developed by Pinsky et al.[39]

2.4. Battery Properties Computations. Voltages were computed directly from a difference in total energy between the lithiated and delithiated state following the methodology presented in Aydinol et al.[40] Entropic contributions were neglected. When the delithiated state still contained lithium in the structure (e.g., $LiV_2(PO_4)_3$), the lithium ordering over the available sites was determined by enumerating possible ordered states of lithium and lithium vacancies using Hart's algorithm and choosing the state leading to the lowest electrostatic energy computed by an Ewald sum on formal valence point charges.[34]

Thermodynamic stability at zero K and zero pressure was evaluated using *ab initio* computed total energies. The stability of any phase was evaluated by comparing it to other phases or linear combination of phases leading to the same composition using the convex hull construction. GGA and GGA+U computations were combined using Jain et al.'s methodology.[41] The stability of any compound was quantified by evaluating the *energy above the hull*, which is the negative energy of the reaction that decomposes a compound into the most stable combination of other phases. When the compound is stable at zero K, its energy above the hull is 0 meV/at. An energy above the hull is always positive, and its magnitude indicates the degree of instability of the compound.

Safety or thermal stability was computed as in Ong et al. by evaluating the oxygen chemical potential necessary for the compound to decompose at equilibrium through oxygen gas evolution.[42] This approach assumes an equilibrium process and an entropic contribution to the reaction solely from the oxygen gas. The oxygen chemical potential reference (μ_{O_2} = 0 meV) is chosen to be air at 298 K, according to the tabulated entropy of oxygen in the JANAF tables and the fitted oxygen molecule energy from Wang et al.[24,43] Oxygen chemical potential ranges (with respect to this reference) can be found for typical binary oxides in the Supporting Information of Hautier et al.'s paper.[37]

2.5. Phosphates Classification. In this work, any compound containing phosphorus atoms tetrahedrally coordinated by oxygen will be considered as a phosphate. We will follow the classification of phosphates from Durif.[44] The first criteria used to classify phosphates is based on the oxygen to phosphorus ratio. Three categories can then be distinguished:

- O/P = 4 orthophosphates or monophosphates
- O/P > 4 oxyphosphates
- 5/2 < O/P < 4 condensed phosphates

The condensed phosphates have the particularity that some PO_4 groups share corners with other PO_4 groups. The condensed phosphates can be subdivided between:

- Linear polyphosphates. They contain groups of PO_4 tetrahedron sharing one or two corners with other PO_4 tetrahedron. The general formula for these is $(P_nO_{3n+1})^{(n+2)-}$. Pyrophosphates (n = 2) $(P_2O_7)^{4-}$ belong to this group. Metaphosphates $(PO_3)^-$ are formed if the chain is infinite.
- Cyclophosphates. They present corner sharing rings of tetrahedron PO_4 and are of formula $(P_nO_{3n})^{n-}$. Among those, the (cyclic) metaphosphates are common $(PO_3)^-$.
- Ultraphosphates. They present PO_4 tetrahedron sharing three of their oxygen with other PO_4 groups. $(P_{2m+n}O_{5m+3n})^{n-}$

3. RESULTS

3.1. Thermodynamical Stability of Phosphates. We analyze the thermodynamic stability at zero K and zero pressure of the known ICSD compounds. For each of those known compounds, the energy above the hull was computed. It should be noted that it is possible for a known compound to be unstable in this analysis (i.e., having a nonzero energy above the hull). Besides possible errors from DFT, some phases present in the ICSD are prepared at high temperature (and sometimes at high pressure conditions), stabilizing a compound that would be unstable at zero K and zero pressure. Moreover, this analysis is purely thermodynamical, and compounds can be synthesized while metastable.

Table 1. Predicted New (with respect to the ICSD database) Stable Phases at Zero K[a]

formula	space group	based on	based on ICSD nb	exp. evidence
$LiSn_2(PO_3)_5$	*Pc*(7)	$LiPb_2(PO_3)_5$	61207	none
$LiSb(PO_3)_4$	*C*2/*c*(15)	$LiYb(PO_3)_4$	67705	none
$LiCr_4(PO_4)_3$	*Pnma*(62)	$Cd_4Na(PO_4)_3$	8115	none
$Li_2Cr(P_2O_7)$	*C*2/*c*(15)	$Li_2Cu(P_2O_7)$	72485	none
$Li_3Mo_2(PO_4)_3$	R$\bar{3}$(148)	$Li_3Fe_2(PO_4)_3$	95973	yes[53]
$LiCo(P_2O_7)$	P 2_1(4)	$LiSc(P_2O_7)$	91496	none
$LiCo(PO_4)$	Pn2_1a(33)	$LiZn(PO_4)$	79352	none
$LiBi(PO_3)_4$	*C*2/*c*(15)	$LiYb(PO_3)_4$	67705	none
$LiCr(P_2O_7)$	P 2_1(4)	$LiSc(P_2O_7)$	91496	ICSD: 240965
$LiMn(P_2O_7)$	P 2_1(4)	$LiFe(P_2O_7)$	63509	ICSD: 415153
$LiMo_2(PO_4)_3$	*P*2_1/*c*(14)	$Li_3Fe_2(AsO_4)_3$	90880	yes[53]
$LiV_2(PO_4)_3$	R$\bar{3}$c(167)	$LiTi_2(PO_4)_3$	95979	none
$LiCo(PO_3)_4$	*Pbcn*(60)	$LiAl(PO_3)_4$	74860	none
$LiFe(PO_3)_4$	*Pbcn*(60)	$LiAl(PO_3)_4$	74860	yes[52]
$LiCr_6(P_2O_7)_2(P_3O_{10})$	*P*2_1/*m*(11)	$NaMn_6(P_2O_7)_2(P_3O_{10})$	280928	none
$LiTi(PO_3)_5$	*P*2_1/*m*(11)	$Na_2Mn(PO_3)_5$	91544	none
$LiV(PO_3)_4$	*Pbcn*(60)	$LiAl(PO_3)_4$	74860	none
$LiTi(PO_3)_4$	*Pbcn*(60)	$LiAl(PO_3)_4$	74860	none
$Li_3Cr_2(PO_4)_3$	R$\bar{3}$(148)	$Li_3Fe_2(PO_4)_3$	95973	yes[53,54]
$Li_9Cr_3(P_2O_7)_3(PO_4)_2$	P$\bar{3}$c1(165)	$Li_9Fe_3(P_2O_7)_3(PO_4)_2$	50958	ICSD:417755
$Li_2Fe_3(P_2O_7)_2$	*P*2_1/*c*(14)	$Li_2Ni_3(P_2O_7)_2$	83662	yes[51]
$LiMn(PO_3)_4$	*Pbcn*(60)	$LiAl(PO_3)_4$	74860	none
$LiMn_2P_3O_{10}$	*P*2_1/*m*(11)	$LiCo_2P_3O_{10}$	83582	none
$LiCo(PO_3)_3$	P $2_12_12_1$(19)	$LiMn(PO_3)_3$	51632	ICSD:153515
$LiCr(PO_3)_4$	*Pbcn*(60)	$LiAl(PO_3)_4$	74860	yes[52]
$LiMo(PO_3)_4$	*Pbcn*(60)	$LiAl(PO_3)_4$	74860	none
$LiMo_2(PO_4)_3$	R$\bar{3}$(148)	$LiSn_2(PO_4)_3$	83832	yes[53]

[a] We indicated the Hermann-Maugin notation and the space group number of the phase along with the formula and number of the ICSD entry on which the new compound is based (e.g., through ionic substitution). Previous experimental evidence refers to that mentioned in the literature without a precise crystal structure assignment and to entries entered after 2006 in the ICSD.

However, it is expected that for existing compounds, any instability from the zero K convex hull should be in a reasonable energy range. Among the 37 compounds containing at least Li, P, O, and a redox active metal, and which are reported with no partial occupancies in the ICSD, only six have a distance to the hull larger than 10 meV/at (see Table 2 of the Supporting Information). Obvious reasons for metastability at zero K could be identified for four of those six compounds. The NASICON $LiV_2(PO_4)_3$ is formed by electrochemical delithiation and was never synthesized directly.[45] The $LiCu(PO_3)_3$ P$\bar{1}$ structure is probably also a metastable compound as it is known to transform to the $LiCu(PO_3)_3$ orthorhombic form upon heating.[46,47] The $LiFePO_4$-β is a high-pressure phase higher in energy than the olivine structure.[48] The energy above the hull of $Li_2Mn_2P_6O_{18}.10H_2O$ is extremely high (400 meV/at), and while it is possible that this lack of stability results from inaccuracy in the representation of water in our database, it is more likely due to a missasignment of the hydrogen positions in the ICSD structure, as is hinted by the large ionic relaxations observed during the DFT computations.[49] With more accurate hydrogen positions, this structure is likely to have a much lower calculated energy. Surprisingly, $LiCoPO_4$ olivine is found to be 24 meV/at above a predicted LISICON structure in which the transition metals are tetrahedrally coordinated.

A similar thermodynamical analysis has been performed for the compounds proposed by the substitution algorithm.[35] Twenty-seven novel phases were found to be on the convex hull and thus computationally stable at zero K. Table 1 shows the thermodynamic data for those compounds. A few compounds have been inserted in the ICSD after 2006 and were not in our working version of this database ($LiCo(PO_3)_3$, $LiCrP_2O_7$, $LiMnP_2O_7$, and $Li_9Cr_3(P_2O_7)_3(PO_4)_2$). $Li_2Fe_3(P_2O_7)$ has recently been synthesized but is not yet entered in the ICSD.[50,51] It is encouraging that in each case the correct crystal structure was found by our compound prediction scheme. A few compounds of formula $LiM(PO_3)_4$ based on the $LiAl(PO_3)_4$ crystal structure are also predicted. Evidence for their synthesis with M = Fe and Cr are presented in Murashova et al.[52] We also predict the existence of two molybdenum compounds with the NASICON-like structure ($Li_3Mo_2(PO_4)_3$ and $LiMo_2(PO_4)_3$). Although not referenced in the ICSD, synthesis of those compounds has been claimed in the literature.[53] Similarly, the $Li_3Cr_2(PO_4)_3$ NASICON is absent in the ICSD but referenced in several papers.[53,54] This demonstrates the ability of a substitution algorithm coupled with a DFT phase stability analysis to discover new phases beyond the ICSD 2006 data set.

3.2. Preferred Local Environments. Our large data set of computed phosphates can be used to study the local environments that each ion favors. Figure 1 plots for each ion in different

dx.doi.org/10.1021/cm200949v |*Chem. Mater.* 2011, 23, 3495–3508

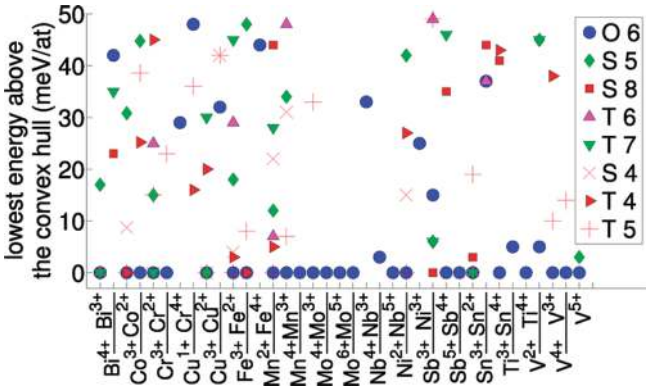

Figure 1. Lowest distance to the convex hull for different coordination environments of each ionic species in our phosphate data set. Each symbol refers to a different local environment: O6, octahedral; S4, square planar; T4, tetrahedral; S5, square pyramidal; T5, trigonal bipyramidal; T7, trigonal prismatic square face monocapped; T6, trigonal; and S8, square antiprismatic. An energy above the hull of 0 meV/at indicates that the environment is found in a compound thermodynamically stable at 0 K.

coordination environments the lowest energy above the hull that is found in our data set. Each symbol indicates a different local environment. Overlap between symbols can happen when two local environments are present in the same compounds or in compounds with similar stability. Zero energy above the hull indicates that at least one stable compound exists with this coordination environment.

The vast majority of transition metals are stable in octahedral environments (blue circles). For some +2 ions such Fe, Mn, and Co, trigonal bipyramidal environments (which can also be seen as distorted square pyramidal environments) exist as well (red crosses). The four ICSD compounds: $Fe_2P_2O_7$, $Ni_2P_2O_7$, $Co_2P_2O_7$, and $Co_3(PO_4)_2$, as well as its predicted isostructural $Mn_3(PO_4)_2$, are all compounds with mixed octahedral and trigonal bipyramidal environments. This type of mixed environment compounds are also observed in lithium-containing phosphates in the recently discovered $Li_2FeP_2O_7$ and $Li_2MnP_2O_7$.[55,56]

Both Cu^{2+} and Cr^{2+} are stable in square planar environments such as in the ICSD $Li_2CuP_2O_7$ compound and the isostructural predicted $Li_2CrP_2O_7$. Mixed octahedral and square planar are also possible such as in $Cu_3(PO_4)_2$.

Larger ions such as Sb^{3+}, Bi^{3+} ,and Sn^{2+} show higher coordination environments (8- or 7-fold coordination). On the contrary, when stable, their oxidized equivalent (e.g., Sb^{5+} and Sn^{4+}) form in octahedral environments because of their smaller size.

Few tetrahedrally coordinated redox active elements are found to be stable in phosphates. Only the trigonal phase of $FePO_4$ contains a Fe^{3+} in a tetrahedrally coordinated environment. No stable tetrahedral redox active element is found in a lithium containing phosphate.

However, tetrahedrally coordinated structures such as the LISICON-like structures formed by $LiZnPO_4$ can be very energetically competitive for some ions such as Fe^{2+} and Mn^{2+} (only 5 to 9 meV/at above the stable olivine structure). For Co^{2+}, we predict the cobalt LISICON $LiCoPO_4$ to be significantly more stable than olivine by 24 meV/at. While it has been shown that other polymorphs can be stabilized under high pressure,[57] they all have octahedrally coordinated Co, and no report of a phase with tetrahedrally coordinated Co exists to the best of our

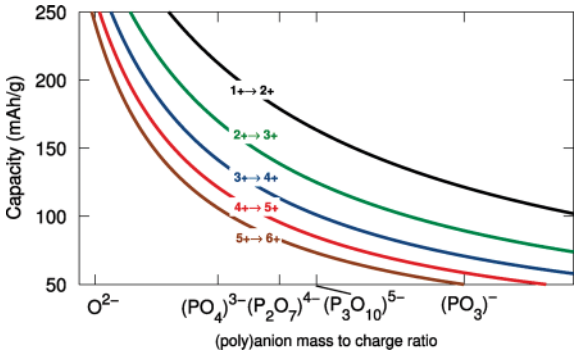

Figure 2. Best achievable gravimetric capacity for different $M^{(n-1)+}/M^{n+}$ couples as a function of the mass-to-charge ratio of the (poly)anion. Oxides and different phosphate polyanions are indicated on the mass-to-charge ratio axis. For the sake of comparison, this plot assumes the mass of iron for the M element.

knowledge (even in low temperature synthesis conditions).[58] To verify the accuracy of this result, we assessed the $LiCoPO_4$ phase stability with GGA with different U values, with the Heyd−Scuseria−Ernzerhof (HSE) hybrid functional and in an antiferromagnetic state (Supporting Information).[26] Even though these additional computations come with some different physical approximations, they all led to the same conclusion placing the LISICON structure lower in energy than the olivine. This theoretical result suggests that a tetrahedral $LiCoPO_4$ might be synthesizable. If direct synthesis is not successful, an alternative synthesis route could be to form $NaCoPO_4$, which is known to form under certain conditions with tetrahedrally coordinated cobalt and perform a Li−Na ion-exchange.[59]

3.3. Capacity Limits in Phosphates. The amount of charge extractable from an electrode material per unit weight is the gravimetric capacity. It is possible to place general bounds on the gravimetric capacity of compounds of formula $Li_xM_yX_z$, where M is a redox active element and X is a (poly)anion. The maximum achievable capacity for a one-electron delithiation process depends on the one-electron couple used (M^{1+}/M^{2+}, M^{2+}/M^{3+},...), the mass of the element M, and the charge to mass ratio for X. For instance, assuming an orthophosphates compound (X = $(PO_4)^{3-}$) and a Fe^{2+}/Fe^{3+} couple, the best capacity achievable is around 170 mAh/g (this corresponds to the $LiFePO_4$ stoichiometry). Figure 2 plots the maximum capacity for different one-electron redox couples (the different colored lines) as function of the charge-to-mass ratio of the (poly)anion X. For the sake of comparison, this plot assumes the mass of iron for the M element, which is a reasonable average for the 3*d* transition metals. Figure 2 highlights the importance of the cation charge and the charge-to-mass ratio on the anion. For a high valent cation redox couple (e.g., M^{5+}/M^{6+}), a large amount of anion mass is required in the compound to compensate, thereby decreasing the specific capacity. Hence, from a specific energy perspective, low valent redox couples, with reasonably high voltage and combined with (poly)anions with high negative charge-to-mass ratio, are optimal. Different classes of phosphates are represented in Figure 2 at different charge-to-mass ratio: orthophosphates (X = $(PO_4)^{3-}$), pyrophosphates (X = $(P_2O_7)^{4-}$), and metaphosphates (X = $(PO_3)^{-}$) (see Methods section for the classification). For comparison, the pure oxides are also indicated on the graph (X = O^{2-}). All the phosphates show lower maximal capacities than the oxides. For instance, for

the couple M^{2+}/M^{3+}, the best achievable capacity for oxides is around 300 mAh/g, while that for the orthophosphates is around 170 mAh/g. Moreover, condensation of the PO_4 groups tends to increase the mass-to-charge ratio and to decrease dramatically the maximal capacity. For the couple M^{2+}/M^{3+}, the capacity is reduced to 100 mAh/g for metaphosphates ($X = (PO_3)^-$).

Oxyphosphates are situated between the oxides and orthophosphates in terms of mass-to-charge ratio and have therefore a higher achievable maximal capacity than ortho or condensed phosphates.

3.4. Voltage Data Mining. *3.4.1. Voltages Range.* The voltage delivered by cathode materials with respect to a certain anode (here lithium metal) is a critical battery property. The voltage influences directly the energy stored per unit mass and volume (i.e., the specific energy and energy density). However, a limit to this voltage is imposed by the electrolyte. Current commercial electrolytes are not stable on long-term cycling above a voltage threshold situated around 4.5 V (versus lithium metal). In this work, all voltages are referenced to lithium metal.

We computed the delithiation voltage for all of the quaternary lithium-containing phosphates in our data set. Only compounds reasonably stable in their lithiated state (energy above hull <50 meV/at) were considered. The amount of lithium removed corresponds to a one-electron oxidation of the redox active element. The delithiation and computational procedure is presented in the Methods section. In total, our data set contains 651 voltage computations, on which we performed statistical analysis.

The first parameter influencing the voltage is the active redox couple.[60] A cathode working on the Ni^{2+}/Ni^{3+} couple is expected to deliver a much higher voltage than one operating on Ti^{3+}/Ti^{4+}. We assumed a normal distribution of the voltages around a different mean for each redox couple. The standard deviation takes into account the effect of the specific crystal structure and is considered common to all couples. The mathematical expression for the fitted normal distribution is

$$V_{M^{(n-1)+}/Mn^{n+}} = N(\mu_{M^{(n-1)+}/M^{n+}}, \sigma) \quad (1)$$

where N represents a normal distribution and $\mu_{M^{(n-1)+}/M^{n+}}$ is the mean value for the $M^{(n-1)+}/M^{n+}$ redox couple. A maximum likelihood fit to the data determined a standard deviation σ of 0.49 V and the mean value for each couple. Figure 3 represents for each redox couple the mean voltage with a bar indicating the range that captures 90% of all compounds with that redox couple. The mean voltage for the ternary oxides present in the ICSD are indicated with red dots for comparison. The 4.5 V voltage limit for current commercial electrolytes stability is indicated by the red dashed line.

The average voltage for each element increases with oxidation state (e.g., the average voltage for Co^{3+}/Co^{4+} is higher than for Co^{2+}/Co^{3+}). The only exception is tin, for which the average Sn^{2+}/Sn^{3+} voltage is higher than Sn^{3+}/Sn^{4+}, indicating that Sn^{3+} is not stable and will disproportionate into Sn^{2+} and Sn^{4+}.

Figure 3 shows that phosphates exhibit higher voltages than oxides for a similar redox couple. This fact is well-known in the battery field and is explained by the inductive effect.[61] The phosphorus ion sharing a common oxygen with the transition metal M, through a M−O−P link, influences the covalency of the M−O bond. The electronegative phosphorus attracts electrons from the oxygen and weakens the covalent metal to oxygen bond. The weaker the M−O covalent bond, the higher the

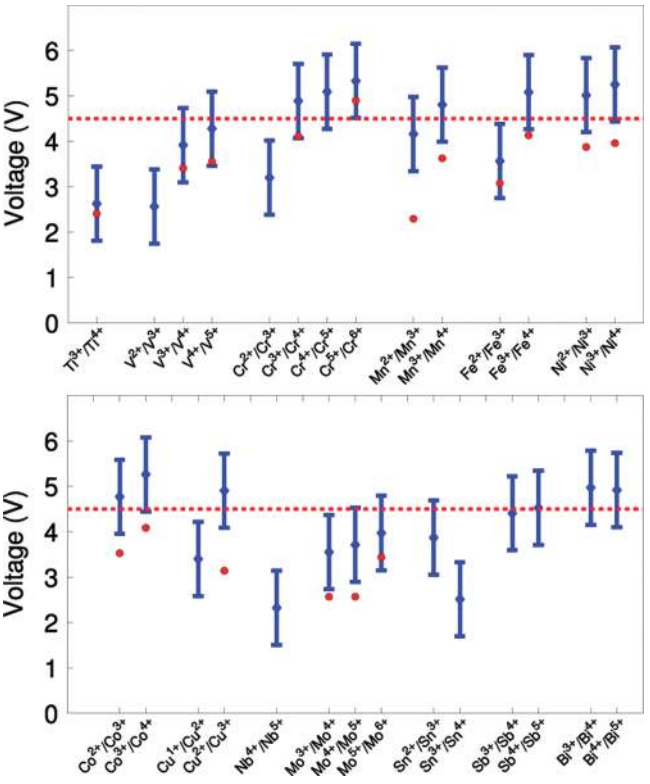

Figure 3. Voltage distribution for different redox couples in phosphates. Red circles indicate the average voltage calculated for all ternary oxides in the ICSD database. The blue bar indicates the range that captures 90% of all phosphate compounds with that redox couple. The red dashed line at 4.5 V indicates the practical electrolyte limit. The couples are sorted by the mass of their element.

voltage for the $M^{(n-1)+}/M^{n+}$ couple. Therefore, the presence of the phosphate group has the effect of increasing the voltage (above that of a "pure" oxide).

Interestingly, according to our data, this inductive effect seems nonuniform across couples. Couples such as Ti^{3+}/Ti^{4+} and Fe^{2+}/Fe^{3+} have small inductive effects, whereas couples such as Mn^{2+}/Mn^{3+} and Mn^{3+}/Mn^{4+} have higher inductive effect. The lack of anion effect observed in the case of titanium Ti^{3+}/Ti^{4+} is consistent with early calculations comparing oxides, sulfides, and selenides[40] but somewhat in contradiction with the phosphate literature. Indeed, the important difference in voltage between lithium insertion in titanium NASICON (2.5 V) and lithium insertion into the spinel-related $Li_4Ti_5O_{12}$ (1.6 V) has been reported as an evidence for the inductive effect.[62] Our data shows to the contrary that on average the inductive effect is not very pronounced for the Ti^{3+}/Ti^{4+} couple. Our average voltage for oxides with titanium is higher than 1.6 V and lies closer to 2.3 V. Lithium insertion in spinel-based structures tends to be low in voltage for structural reasons. Lithiating $Li_4Ti_5O_{12}$ creates very strong electrostatic Li^+-Li^+ interactions, which reduces the intercalation voltage, and the focus of the comparison on insertion in $Li_4Ti_5O_{12}$ has somewhat biased the analysis in the literature. Lithiation of TiO_2 anastase proceeds at a higher voltage (slightly lower than 2 V),[63] and ramsdellite $LiTi_2O_4$ has recently been reported experimentally as deintercalating at a even higher potential (2 to 2.5 V).[64] Both those results are much closer to our computed average voltage.

dx.doi.org/10.1021/cm200949v |*Chem. Mater.* 2011, 23, 3495–3508

The inductive effect is one of the motivations for the interest in polyanionic systems. Couples often too low in voltage in oxides, such as Mn^{2+}/Mn^{3+}, V^{3+}/V^{4+}, or Fe^{2+}/Fe^{3+}, can be higher than 3 V in phosphates. However, this effect can be detrimental for certain couples. For instance, Mn^{3+}/Mn^{4+}, Co^{3+}/Co^{4+}, Ni^{2+}/Ni^{3+}, and Ni^{3+}/Ni^{4+}, while used in commercial oxide-based lithium ion batteries, are too high in voltage to be of interest in phosphates with the current electrolyte technology.

Before comparing our results to the experimental literature, we should note that our data set consists only of voltages obtained from the delithiation of rather stable lithiated compounds. No voltage from lithium insertion in stable compounds is used. There is a technological justification for this choice. As the standard commercial anode (carbon) is made without lithium, there is a need for the cathode to be the lithium source of the battery. This choice influences somewhat the obtained voltage range. Voltages obtained from lithium *insertion* into stable compounds are usually lower than voltages obtained by *delithiation* of stable compounds (in similar chemistries and activating the same redox couple). Indeed, as the voltage is the difference between the energy of the charged and discharged state, inserting Li in stable compounds will lead in general to lower voltage than delithiating stable compounds. For instance, the Fe^{2+}/Fe^{3+} redox couple can be activated in pyrophosphate by inserting lithium into the stable $LiFeP_2O_7$ or by removing lithium from the stable $Li_2FeP_2O_7$. The crystal structures for those two compounds are different, and the lithium insertion into the stable charged state in $LiFeP_2O_7$ is measured to be 2.9 V,[61] while the delithiation voltage from the stable discharged state $Li_2FeP_2O_7$ is higher at 3.5 V.[55]

The Fe^{2+}/Fe^{3+} couple has been well studied in phosphates. This couple is reported at 2.8 V for insertion in $LiFe_2(PO_4)_3$ NASICON, at 2.9 V for insertion into $LiFeP_2O_7$, at 3.1 V in amorphous $Fe_4(P_2O_7)_3.4H_2O$,[61] and at 3 V in the high-pressure form of $FePO_4$.[65] The higher voltage of 3.5 V in olivine $LiFePO_4$ seems to be unusual among this data set but is close to our computed average. More recent experimental results on delithiation compounds working on the Fe^{2+}/Fe^{3+} couple such as $Li_2FeP_2O_7$ at 3.5 V,[55] $Li_2Fe_3(P_2O_7)_2$ at 3.4 V,[50] and $LiFe_2(P_3O_{10})$ at 3.2 V[66] indeed show higher voltages.

The Ti^{3+}/Ti^{4+} couple has been identified around 2.5 V when inserting into the NASICON structure: $LiTi_2(PO_4)_3$.[67,68] A potential at 2.6 V is found for insertion into TiP_2O_7.[62] Hydrogenated phosphates as $Ti(HPO_4)$ have also been inserted at a voltage around 2.5 V.[69] All those experimental results fit well with our computed average of 2.6 V for Ti^{3+}/Ti^{4+}.

The Mn^{2+}/Mn^{3+} couple is less studied with a strong focus on $LiMnPO_4$ measured at 4.1 V.[5] Recent results on $Li_2Mn(P_2O_7)$ showed a voltage around 4.5 V.[56] Both voltages lie in our predicted voltage range.

Experimental measurements of redox active chromium in phosphates is scarce. Patoux et al. mention the inactivity of the Cr^{2+}/Cr^{3+} couple in the $Li_3Cr_2(PO_4)_3$ and $Li_1TiCr(PO_4)_3$ NASICONs.[54] A claimed measurement through cyclic voltametry of the Cr^{3+}/Cr^{4+} couple in $LiCrP_2O_7$ between 3.1 and 3.5 V seems extremely low but would correspond with our voltage range for Cr^{2+}/Cr^{3+}.[70] The data might have been wrongly interpreted as a measurement of the voltage during delithiation, while the actual process was a lithium insertion into $LiCrP_2O_7$.

Vanadium is an extensively studied element in phosphates. The V^{2+}/V^{3+} couple is reported in NASICON at 1.7 V[60] and at 2 V for $LiVP_2O_7$.[62] Both lie in our voltage range but on the lower side. The V^{3+}/V^{4+} couple has been studied experimentally in many different structures from the $Li_3V_2(PO_4)_3$ monoclinic (3.8 V)[7,45] and rhombohedral (3.8 V)[71] NASICON to the pyrophosphate $LiVP_2O_7$ (4.1 V).[62] All those experimental results are in agreement with our predicted voltage range. An outlier is found in $Li_4VO(PO_4)_2$ inserting at 1.5 V, indicating most likely a significant polarization.[72] The position of the V^{4+}/V^{5+} couple, on the other hand, has been more polemical in the experimental literature. Our computations locate the couple on average at 4.2 V. However, extraction of the last lithium in the NASICON ($Li_1V_2(PO_4)_3 \rightarrow V_2(PO_4)_3$), which requires the oxidation of vanadium to +5 was believed early on to occur at a potential higher than 4.5 V.[73] More recent experimental results show a significant hysteresis between the charge and discharge of the last lithium in NASICON with a charge around 4.6 V but a discharge much lower at 4.1 V.[7] A mechanism based on charge-ordering asymmetry has been proposed by Yin et al. to explain this behavior.[45] The activity of V^{4+}/V^{5+} in other compounds such as in the three polymorphs of $LiVOPO_4$ oxyphosphates, α (3.7 V),[74] β (4 V),[75] ε (4 V),[76] and $LiVOP_2O_7$ (4.1 V)[77] are all in agreement with our computational voltage range.

There is less data for high voltage couples as issues with electrolyte decomposition often obscure delithiation. The high voltage electrochemical tests reported for the nickel and cobalt olivines confirm the high voltage associated with the two Co^{2+}/Co^{3+} and Ni^{2+}/Ni^{3+} couples. $LiNiPO_4$ has been measured at 5.2 V[78] and $LiCoPO_4$ at 5.0 V and 4.8 V.[79,80] Some experimental results have recently appeared on the Mn^{3+}/Mn^{4+} couple. Those experimental results based on $LiMnPO_4$ doped with Mg (4.8 V),[81] and on $Li_2Mn(P_2O_7)$ (5.3 V)[56] confirm the high voltage computed for this couple. Our computations can provide an explanation for some unsuccessful electrochemical delithiation attempts. For instance, $LiCo(PO_3)_3$ was tested electrochemically up to 5 V but did not show any activity as expected for the high voltage of the Co^{3+}/Co^{4+}.[82] Similarly, the failed attempt to extract lithium from $LiFeP_2O_7$ can be attributed to the high voltage of the Fe^{3+}/Fe^{4+} couple.[83]

We predict the average voltage for the Mo^{3+}/Mo^{4+}, Mo^{4+}/Mo^{5+}, and Mo^{5+}/Mo^{6+} couples to lie exactly in the 3−4.5 V voltage window. It is therefore surprising that very few experimental

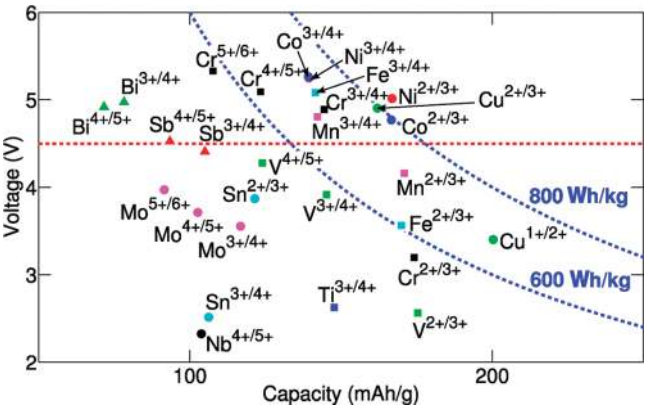

Figure 4. Mean voltage in phosphates versus maximum gravimetric capacity achievable. Specific energy curves at 600 and 800 Wh/kg are drawn on the figure (blue dashed lines). The red dashed line indicates the upper voltage which we consider safe against decomposition of the electrolyte. Different colors and markers have been used for different elements.

dx.doi.org/10.1021/cm200949v |*Chem. Mater.* 2011, 23, 3495–3508

reports on molybdenum electrochemistry in phosphates have been published. To our knowledge, only lithium insertion in $(MoO_2)_2P_2O_7$ has been reported at 2.6 V.[84] Unfortunately, the experimental results indicate amorphization during lithiation and are difficult to compare to computations which assume topotactic insertion.

3.4.2. Specific Energy Analysis. The data mining of the voltage (Figure 3) can be used in conjunction with our previous analysis on best gravimetric capacities achievable (Figure 2) to detect couples that may lead to interesting specific energies. Figure 4 plots the mean voltage for each couple with respect to the best achievable capacity in a phosphate (excluding oxyphosphates) as computed in section 3.3 and in Figure 2. The specific energy is the product of the voltage and the capacity; specific energy curves at 600 and 800 Wh/kg are drawn on the figure (blue dashed lines). The red dashed line indicates the upper voltage that we consider safe against decomposition of the electrolyte. For comparison, the theoretical specific energy of $LiFePO_4$ olivine is 600 Wh/kg.

Using this plot, couples such as Sn^{3+}/Sn^{4+}, Mo^{3+}/Mo^{4+}, Mo^{4+}/Mo^{5+}, Mo^{5+}/Mo^{6+}, Sb^{3+}/Sb^{4+}, and Sb^{4+}/Sb^{5+}, while of interest for their voltages, have to be excluded (as one-electron systems) because of their high atomic weights. The one-electron redox couples that are likely to improve the gravimetric specific energy over $LiFePO_4$ (600 Wh/kg) and are below 4.5 V are the Fe^{2+}/Fe^{3+}, Mn^{2+}/Mn^{3+}, and Cu^{1+}/Cu^{2+} couples. While there is extensive work on the two first couples in $LiFePO_4$ and $LiMnPO_4$, to our knowledge there has been no experimental work on phosphate Cu^{1+}/Cu^{2+} compounds. The Cu^{1+}/Cu^{2+} couple not only exhibits a voltage likely to fit in our targeted voltage window, but also benefits from a higher achievable capacity because of its low oxidation state (Figure 2).

It is challenging to find a one electron phosphate compound competitive in terms of specific energy and located in the 3−4.5 V voltage window. The remaining strategy to increase the specific energy is to consider two-electron couples. Both of the couples present in the two-electron transition should both lie in the 3−4.5 V window. From Figure 4, molybdenum (with three couples in the voltage window: Mo^{3+}/Mo^{4+}, Mo^{4+}/Mo^{5+}, and Mo^{5+}/Mo^{6+}) and vanadium (two couples: V^{3+}/V^{4+} and V^{4+}/V^{5+}) are the only two elements with acceptable two-electron voltages. The heavier weight and lower voltage for molybdenum compounds compared to those of vanadium argues against them. For instance, while we predict a molybdenum $Li_3Mo_2(PO_4)_3$ NASICON to be stable, its specific energy (532 Wh/kg) compared to the theoretical specific energy for the vanadium NASICON (722 Wh/kg) is 25% lower.

Among the nontransition metals, we notice that Sb^{3+}/Sb^{5+} is a two-electron redox couple that should be considered, even though the weight of antimony mitigates the benefit of using a two-electron system.

Experimental effort is ongoing in finding phosphates capable of activating two electrons using a M^{2+}/M^{4+} couple. For instance, $Li_2M(P_2O_7)$ (M = Fe, Mn, V) has recently been targeted as a two-electron system with the promise of high capacity.[55,56] Our voltage analysis indicates, however, that it will be extremely difficult to find a two electron M^{2+}/M^{4+} phosphate compound with the current electrolyte technology. From all the possible couples, either the M^{2+}/M^{3+} couple is too low (e.g., V^{2+}/V^{3+}), the M^{3+}/M^{4+} couple is too high (e.g., Mn^{3+}/Mn^{4+}, Fe^{3+}/Fe^{4+}, Cr^{3+}/Cr^{4+}), or both couples are too high (e.g., Ni^{2+}/Ni^{3+} and Ni^{3+}/Ni^{4+}).

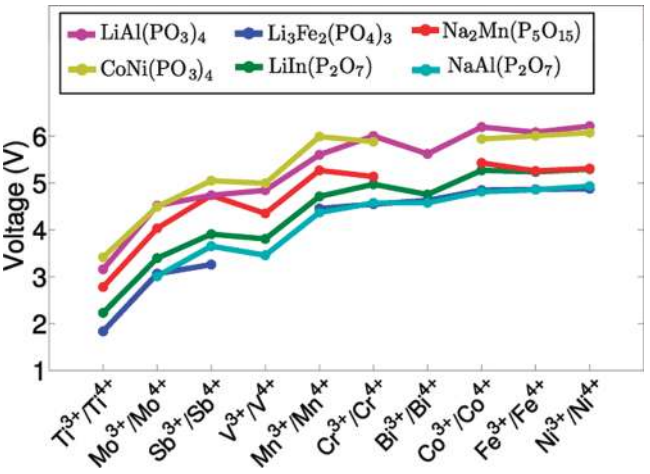

Figure 5. Computed voltage for different redox couples in six different crystal structure prototypes. Each color represents a different crystal structure prototype. The prototypes are labeled by one of the compounds that forms this crystal structure prototype as indicated in the ICSD. The rank in voltage is preserved across different redox couples. High or low voltages crystal structures are the same for all redox couples.

3.4.3. Factors Determining the Voltage. The considerable spread of the voltage around its average for a given redox couple can be related to the effects of the crystal structure. Padhi et al. previously studied the influence of the crystal structure on four different Fe^{2+}/Fe^{3+} phosphate cathode materials.[2]

To investigate the effect of structure, we calculated many of the couples in seven different crystal structures. Figure 5 plots the voltage obtained for different redox couples (all +3/+4 couples) and for seven different crystal structure prototypes. Each colored line corresponds to a different structure prototype. Each prototype is labeled by a compound that forms this crystal structure as given in the ICSD database. Across the different couples, the voltage ranking between crystal structures is conserved: the high voltage and low voltage prototypes are similar for all redox couples. For instance, the purple line in the figure shows the voltages in the structure type of $LiAl(PO_3)_4$. Those compounds tend to be very high in voltage. On the other hand, the light blue line, related to compounds isostructural with $NaAl(P_2O_7)$, is very low in voltage. Moreover, the spread between the highest voltage structure and the lowest one is rather equivalent between redox couples confirming our previous assumption of a common standard deviation among couples.

A statistical view on the influence of prototype and redox couple on the voltage versus lithium anode can be obtained using an analysis of variance (ANOVA).[85] The ANOVA analysis is a statistical tool used to determine if one or several given factors are statistically influencing a variable and how much of the variable variance can be explained by this factor.

The ANOVA analysis relies on the assumption that a voltage k for a given redox couple i and a given crystal structure prototype j can be modeled as

$$V_{ijk} = \mu + \alpha_i + \beta_j + \varepsilon_{ijk} \quad (2)$$

where μ is a constant, α_i represents the deviation to μ due to the redox couple, β_j indicates the deviation to μ due to the crystal structure prototype, and ε_{ijk} is a normally distributed disturbance. We used the ANOVA analysis to evaluate if the chemistry and the crystal structure are statistically significant in determining the

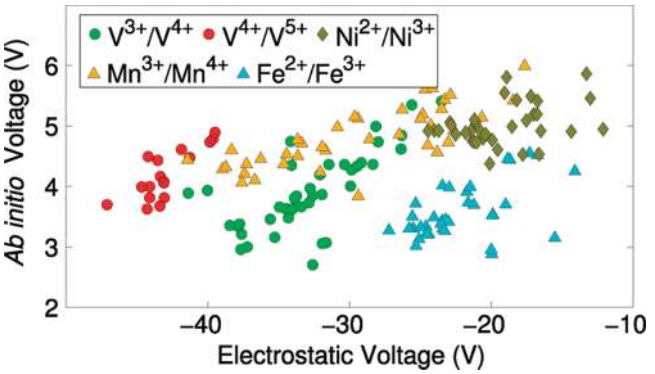

Figure 6. *Ab initio* computed voltage as a function of the voltage computed by electrostatics alone. The electrostatic term was computed using an Ewald sum on the *ab initio* relaxed structure. The different colors indicate different redox couples. While redox couples span different range of voltages, the highest electrostatic voltages correspond to the highest *ab initio* voltages.

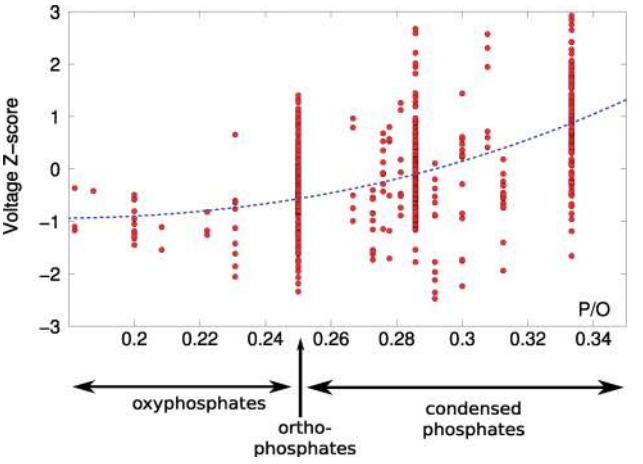

Figure 7. Voltage Z-score in function of the phosphorus-to-oxygen ratio (P/O). The different regions of the phosphates classification, oxyphosphates, orthophosphates, and condensed phosphates, are indicated. Higher phosphorus-to-oxygen ratio are correlated with higher voltages. The blue dashed line is to aid the eye.

voltage and how much of the variance observed in the computed voltages these two factors can explain.

Not surprisingly, performing this ANOVA analysis shows that both redox couple (chemistry + oxidation state) and crystal structure have a significant statistical influence on voltage (both with a high statistical significance of $P < 0.0001$, see Supporting Information). The total variance can be estimated to be 47−66% from the redox couple and 21−33% from the crystal structure. Hence, the majority of the observed variance can be explained by a combination of the redox couple and the crystal structure prototype, as previously observed computationally by Arroyo-de Dompablo et al.[86]

It is of interest to not only relate the voltage to structure prototype but also to understand what particular structural factors influence the voltage. In ionic compounds such as phosphates, the electrostatic energy should influence the energetics and therefore the voltage.[61] To test this hypothesis, we computed an "electrostatic voltage" by computing the voltage obtained by the difference in electrostatics through a simple Ewald summation on the formal charges. Figure 6 plots the *ab initio* computed voltage versus this electrostatic voltage for a few redox couples. While there is significant scattering, a relation can be observed: the higher the electrostatic voltage, the higher the *ab initio* voltage.

To discover what other factors influence the voltage besides the redox couple and the electrostatics, we used the Z-score (or standard score) defined as

$$Z = \frac{V - \mu_{M^{(n-1)+}/M^{n+}}}{\sigma} \qquad (3)$$

where V is a voltage, $\mu_{M^{(n-1)+}/M^{n+}}$ is the mean of the active redox couple, and σ is the voltage standard deviation. Converting to the Z-score allows the different redox couples to be compared on the same footing. To investigate whether other factors have statistically significant effects on the voltage, one can plot the Z-score versus this factor.

A factor often used to rationalize differences in voltages for the same redox couple in phosphates is the inductive effect. Gaubicher et al., for instance, used the number of PO_4 groups linked to the redox active element to rationalize differences in voltages between different crystal structures at the same couple. The lower voltage observed for V^{4+}/V^{5+} during delithiation of $LiVOPO_4$ compared to that of the NASICON delithiation was explained by the smaller number of PO_4 groups connecting the vanadium octahedron for the oxyphosphate (four links) compared to the NASICON (six links).[6] The analysis of our data set did not show any influence of the numbers of PO_4 groups linked to the redox active element (Supporting Information).

Padhi et al., on the other hand, used the length of the P−O bond connected to the redox active element as an indicator of a more or less pronounced inductive effect and used this parameter to rationalize the difference in voltages between four phosphate cathodes working on the Fe^{2+}/Fe^{3+} couple.[61] We found that a relation between the voltage and the P−O bond length does indeed exist (Supporting Information).

The inductive effect can be also estimated by the phosphorus-to-oxygen ratio. More phosphorus compared to oxygen should provide a higher inductive effect. Figure 7 plots the Z-score in function of the phosphorus-to-oxygen ratio. The orthophosphates, condensed phosphates, and oxyphosphates are indicated on the P/O axis. The amount of phosphorus present in the compound influences the voltage, with higher voltages observed for higher P/O ratio, but the scatter is significant. Condensed phosphates have slightly higher voltages than orthophosphates, which are themselves higher in voltages than oxyphosphates.

Using an ANOVA model combining redox couple, electrostatics, and phosphorus-to-oxygen ratio, the three factors were shown to be statistically significant. This analysis attributes 76% of the variance for the redox couple, 6% for the electrostatics, and 4% for the phosphorus-to-oxygen ratio (Supporting Information).

3.5. Phosphates Volumetric Capacity and Energy Density.

Volumetric quantities are as important as gravimetric ones for certain battery applications (e.g., portable electronics). In addition, volumetric energy densities are linked more directly to the price per energy stored than specific energy.[87]

Using our data set, we plotted in Figure 8 the volumetric capacity versus the gravimetric capacity for phosphates (red circles). A linear regression curve can be fitted to this data (red line), showing an average density for phosphates around 3.1 kg/l. For comparison, the theoretical energy densities of the oxides present

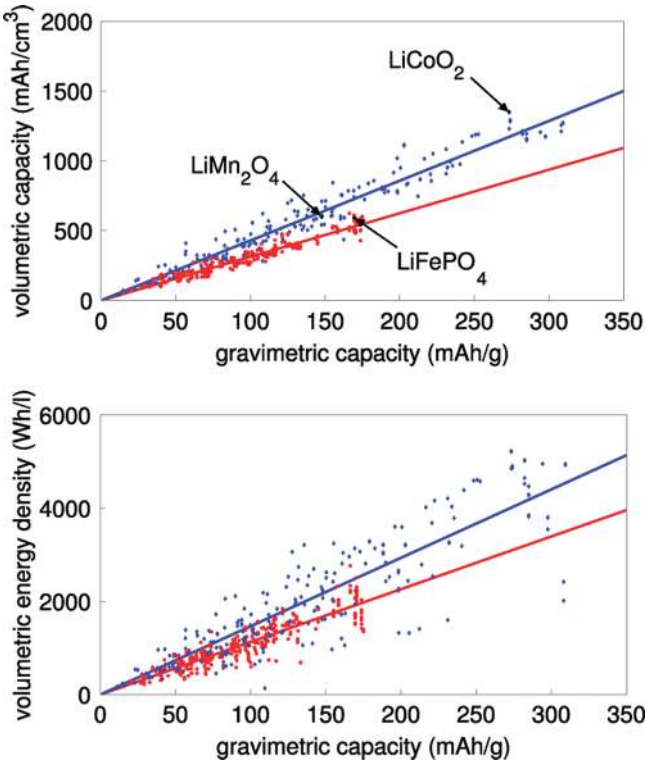

Figure 8. Volumetric capacity and energy density as a function of the gravimetric capacity for oxides (blue diamonds) and phosphates (red circles). Linear regression curves have been plotted in blue for the oxides and red for the phosphates. Only one-electron systems with voltage lower than 4.5 V and relatively stable in the lithiated state (<50 meV/at above hull) have been considered in the analysis. The theoretical volumetric and gravimetric capacities for three current cathode materials, $LiFePO_4$, $LiMn_2O_4$ spinel, and $LiCoO_2$ layered, are indicated in the graph.

in ICSD (obtained by DFT) are plotted in blue diamond with a linear fit (blue curve). The theoretical volumetric and gravimetric capacities for three current cathode materials, $LiFePO_4$, $LiMn_2O_4$ spinel, and $LiCoO_2$ layered, are also indicated in the graph. Only one-electron systems were considered in this plot.

As discussed previously, one-electron oxides can reach higher gravimetric capacities than phosphates (up to 300 mAh/g versus 170 mAh/g for phosphates). In addition, for a similar gravimetric capacity, oxides tend to exhibit higher energy density. This is due to a higher density for oxide materials in comparison to phosphates. This difference in density is linked to the difference in crystal structures formed by phosphates and oxides. Oxides generally form close-packed structures, whereas phosphates tend to be stable in open frameworks such as NASICONs. In our data set, for the same gravimetric capacity, the oxides will have on average a 37% higher volumetric capacity. Among the phosphates, the olivine structure is actually very dense, leading to volumetric capacities around 600 mAh/cm^3. It would be difficult to obtain denser phosphate materials than the olivine compounds. The only option to improve the energy density in one-electron phosphates compared to $LiFePO_4$ would be to use an equivalently dense structure but to increase the voltage. If $LiMnPO_4$ olivine full capacity could be realized, its energy density (2224 Wh/l) would indeed be slightly higher than that

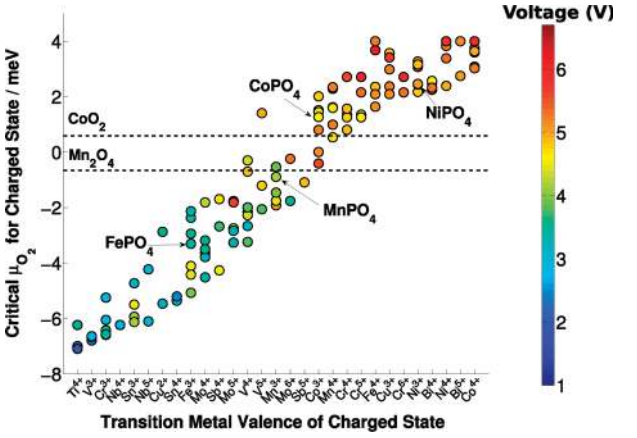

Figure 9. Critical oxygen chemical potential of the charged cathode as a function of the transition metal valence state for the phosphates investigated. The color of each circle represent the voltage. When multiple charged compounds have the same transition metal valence and critical oxygen chemical potential, the voltage was averaged over them in order to keep the graph legible. The red color represents higher voltages, while the blue color represents lower voltages. The ions are sorted by their critical oxygen chemical potential starting with the safest ions. All values at $\mu_{O_2} = 4$ eV represent values higher or equal to 4 eV.

of $LiFePO_4$ (2061 Wh/l) due to the higher voltage and comparably (but slightly lower) density.

While comparing energy density of oxides and phosphates, we should take into account the higher average voltage in phosphates due to the inductive effect. Panel (b) of Figure 8 plots the *energy density* versus the *gravimetric capacity* for our data set. As expected, the higher voltage of phosphates makes the phosphate and oxide curves closer than when comparing capacities. It also increases the spread. Some cathode phosphates get competitive in terms of volumetric energy densities. For instance, a $LiCoPO_4$ in the *Cmcm* structure (based on the high-pressure crystal structure of $LiNiPO_4$ and $LiFePO_4$) exhibits a voltage just below the cutoff at 4.4 V and a rather good volumetric capacity (624 mAh/cc). This would lead to a very high volumetric capacity of 2765 Wh/l. This β-$LiCoPO_4$ phase has been synthesized by high-pressure methods,[57] and it is not surprising to find higher density in high-pressure phases. Unfortunately, currently known high-pressure phosphate phases have suffered so far from low lithium mobility (e.g., in β-$LiFePO_4$).[65] However, on average, the voltage increase is not strong enough (especially if only voltages lower than 4.5 V are taken into account) to compensate for the difference in densities between oxides and phosphates. For the same gravimetric capacity, an oxide has typically an energy density 30% higher than a phosphate.

3.6. Safety and Thermal Stability. Safety is one of the key considerations in the design of lithium-ion battery cathodes. Charged cathodes can be a safety hazard. A typical runaway reaction in a Li battery starts by an overheating event (e.g., caused by an internal or external short) that causes a chain reaction of exothermic processes, typically initiated on the anode side, but a critical process is the ability of the charged cathode to release oxygen and combust the flammable organic electrolyte, ultimately leading to fire.[88,89] Safe battery materials require a thermally stable cathode, as well as a nonflammable electrolyte that is electrochemically stable within the operating range of the battery.

In this work, we focus on the contribution of a phosphate cathode to the thermal stability. We analyzed the safety of the phosphates by calculating the critical oxygen chemical potential at which the charged (delithiated) cathode begins to evolve oxygen gas (henceforth referred to as μ_{O_2}) as predicted by first principles calculations. This methodology was described in greater details in our previous work that investigated the thermal stability of $LiMnPO_4$ and $LiFePO_4$.[42] It should be noted that in the present work, we only studied the equilibrium critical μ_{O_2}. No consideration has been given to possible kinetic barriers to decomposition, which could be important for some compounds.

Figure 9 shows the critical chemical potential at which oxygen would be released from a charged cathode, as a function of the redox active ion in all the phosphates investigated. The lower the critical μ_{O_2}, the more stable the charged cathode is, as a more reducing environment (i.e., higher temperature for a given oxygen partial pressure) is required to cause the cathode to evolve oxygen gas. For reference, the critical μ_{O_2} for the charged cathodes of existing lithium battery cathodes in commercial production, CoO_2 (fully charged $LiCoO_2$) and Mn_2O_4 (charged $LiMn_2O_4$), are labeled, as well as some of the promising olivine phosphates with significant research interest. The thermal stability of charged $LiCoO_2$ is well known to be a significant safety concern.[90] The plot also shows the average voltage associated with the ion.

A significant spread of the critical oxygen chemical potential exists for a given ion. Indeed, depending on the exact position of the phase in the phase diagram and of its competing phases, the oxygen chemical potential can be quite different. General conclusions can however be made for each of the ions and, if we consider a material with an oxygen chemical potential lower than Mn_2O_4 delithiated spinel to be safe, the safe ions are Ti^{4+}, V^{3+}, Cr^{3+}, Nb^{4+}, Sn^{3+}, Nb^{4+}, Cu^{2+}, Sn^{4+}, Fe^{3+}, Mo^{4+}, Sb^{4+}, Mo^{5+}, V^{4+}, V^{5+}, Mn^{3+}, Mo^{6+}, and Sb^{5+}.

Figure 9 shows also that high voltages are associated with unsafe, high oxygen chemical potential materials. Huggins already suggested this relation between safety and voltage for oxides and conversion reactions.[91,92]

Our computations are in agreement with the well-known exceptional thermal stability of the Fe^{3+} in delithiated $LiFePO_4$.[93] In addition, DSC experiments on $LiV_2(PO_4)_3$ showed a better thermal stability for this V^{4+} phosphate than that for Mn_2O_4 delithiated spinel, in agreement with our computations.[8]

Of the three alternative olivine compounds being heavily researched $LiMPO_4$ (where M = Mn, Co, Ni), all are computed to be significantly less thermally stable than $LiFePO_4$. The thermal instability of charged $LiMnPO_4$ has already been discussed at length in our previous work and experimental works by Kim et al. and Richardson et al.[42,94,95] Our analysis shows that both $LiNiPO_4$ and $LiCoPO_4$ have even worse thermal stability than that of $LiMnPO_4$. Bramnik et al. had previously found experimentally that delithiated $CoPO_4$ released oxygen at a relatively low temperature of 100−200 °C.[96] On the other hand, Okada et al. found that $Li_{0.17}CoPO_4$ decomposes at 280 °C, which is higher than the 200 °C for charged $LiCoO_2$.[97] Regardless of the disagreement, temperatures found in both works are significantly lower than for delithiated $LiFePO_4$. Preliminary experimental results by Wang et al. show that $LiNiPO_4$ decomposes immediately to $Ni_2P_2O_7$ and oxygen gas upon delithiation at room temperature.[98] The predictions from our phase diagrams support both of these experimental observations. [Bramnik et al. reported $Co_2P_2O_7$ and oxygen gas to be the decomposition product for the reduction of $CoPO_4$, which differs from our computed prediction ($Co_3(PO_4)_2$, $Co(PO_3)_2$ and oxygen gas). However, the computed $Co_2P_2O_7$ is only 1 meV/at less stable than a combination of $Co_3(PO_4)_2$ and $Co(PO_3)_2$, which is well within the error tolerance we expect from our DFT calculations.] This result is of technological significance as those Co and Ni olivines are sometimes considered as possible high voltage, high energy density cathode materials, and our work identifies that they are associated with major intrinsic safety concerns.[87]

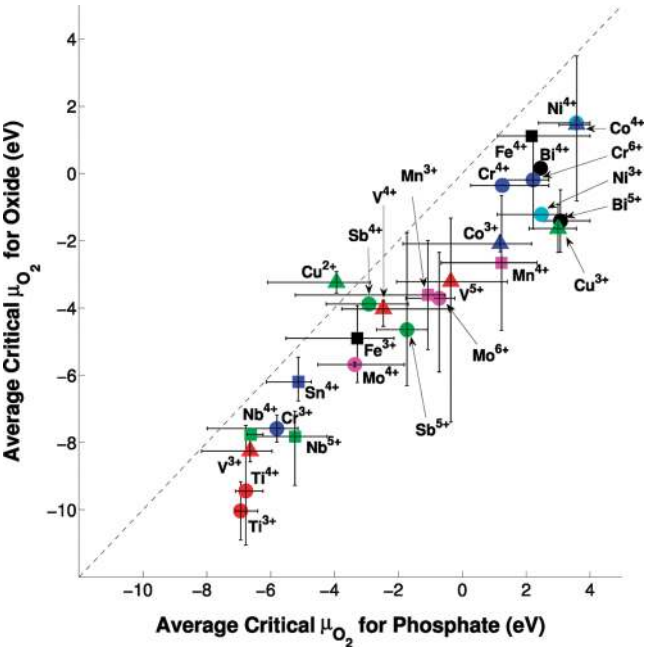

Figure 10. Critical oxygen chemical potential (μ_{O_2}) for oxides versus phosphates with the same oxidation state of active ion. The data points correspond to an average of our data set, and the error bar shows the minimum and maximum values observed. Different colors and markers have been used for different elements.

Phosphates in the olivine structure and phosphates in general have been often claimed to be intrinsically safer materials than oxides.[66,99−103] The rationalization behind the intrinsic phosphate thermal stability invokes the strength of the phosphorus−oxygen bond. As this P−O bond is strong, it is rationalized that it should be very difficult to remove oxygen from a phosphate compound to form the reduced product(s). To test this statement computationally, we compared in Figure 10 the critical oxygen chemical potential for oxides and phosphates as a function of the oxidation state of their redox active ion.

The prevalence of points below the diagonal in Figure 10 indicates that most of the phosphates do actually have a similar or worse thermodynamic thermal stability than oxides for the same oxidation state.

At equilibrium, the argument for the stability of phosphates based on the difficulty to break a P−O bond is not valid. Indeed, this argument would only hold if some dangling P bond would be present in the reduced products. However, the most common oxygen evolution reaction from phosphates involves forming oxygen gas and accommodating the loss of oxygen in the phosphate structure by forming condensed phosphates (e.g., pyrophosphates or metaphosphates). This is, for instance, what happens in many olivine compounds: $2\ MPO_4 \rightarrow M_2P_2O_7 + 1/2O_2$

One of the ions with the largest difference between its critical oxygen chemical potential in oxides and phosphates is Mn^{4+},

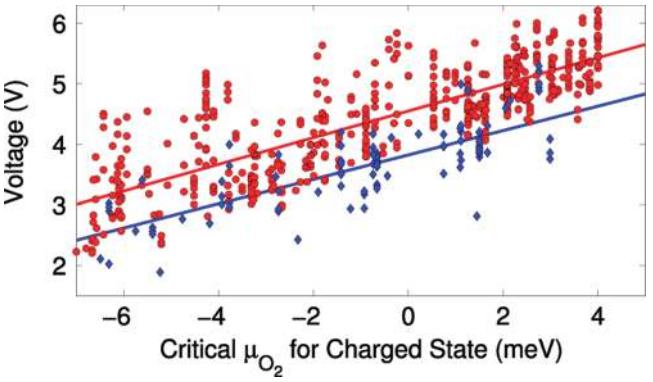

Figure 11. Voltage versus oxygen critical chemical potential (μ_{O_2}) for charged ICSD oxides (blue diamonds) and charged phosphates from our data set (red circles). Linear regressions have been added to the plot to outline the general trends.

which is disproportionally more stable in an oxide. For instance, comparing the critical oxygen chemical potential of MnP_2O_7 and Li_2MnO_3, the phosphate releases oxygen at $\mu_{O_2} = 0.5$ eV (i.e., will be unstable in air at 298 K) and the oxide releases oxygen at a much lower $\mu_{O_2} = -5$ eV. This difference is striking as Mn^{4+} is used as a stabilizer improving thermal stability in some oxides layered compounds.[104]

The thermal stability of a compound is more driven by the oxidation state of the transition metal than by the presence of a P−O bond. For instance, Fe^{3+} is a very thermally stable ion in both oxides and phosphates (in average, $\mu_{O_2} = -5$ eV in oxides and $\mu_{O_2} = -4$ eV in phosphates). However, in phosphates, the Fe^{2+}/Fe^{3+} couple benefits from the inductive effect and is significantly higher in voltage than in oxides. This tendency is general and while for the same oxidation state phosphates are not more thermally stable than oxides, phosphates can provide a higher voltage for an equivalent safety. This is illustrated in Figure 11, where the voltage is plotted versus the critical oxygen chemical potential of the charged cathode. The red circles are phosphates, and the blue diamonds are ICSD oxides. Two regression lines have been added to indicate the general trend. As observed by Huggins, the general tendency for a higher voltage to be associated with higher critical chemical potential is present for both oxides and phosphates.[91,92] However, phosphates present in general a higher voltage for a similar thermal stability. On average, we found phosphates to be around 0.5 V higher in voltage for a similar thermal stability.

Our computations only measure the thermodynamic driving force for oxygen release and different chemistries may have somewhat different kinetics. While kinetics probably controls the oxygen release of the materials that decompose at very low temperature (i.e., the very unstable materials) to be viable, cathodes have to be stable up to 200 °C and higher.[89] At such temperatures, thermodynamic control is more likely.

4. DISCUSSION

In this work, we used high-throughout *ab initio* computations to explore the properties of phosphate compounds as lithium-ion battery cathode materials. The intrinsic limits and expected range of important battery properties, stability, capacity, voltage, and safety, have been analyzed as well as some of the factors influencing them.

The maximum achievable *gravimetric capacity* for a phosphate is smaller than for an oxide because of the lower negative charge per unit wight for the $(PO_4)^{3-}$ anion. The higher the phosphorus content and the degree of condensation of the phosphate groups, the lower the achievable capacity becomes.

The lower densities from phosphate compounds lead to on average 37% lower volumetric capacity compared to that of oxides. The higher voltage achievable in phosphates only slightly mitigates the impact on the energy density, which is on average 30% below that of oxides with the same capacity.

Our work identifies statistically V^{3+}/V^{4+}, V^{4+}/V^{5+}, Cr^{2+}/Cr^{3+}, Mn^{2+}/Mn^{3+}, Fe^{2+}/Fe^{3+}, Cu^{1+}/Cu^{2+}, Mo^{3+}/Mo^{4+}, Mo^{4+}/Mo^{5+}, Mo^{5+}/Mo^{6+}, Sb^{3+}/Sb^{4+}, and Sb^{4+}/Sb^{5+} as the redox couples of interest for phosphate-based cathodes in current electrolyte technology (above 4.5 V). The inductive effect is observed in our data set with higher voltages identified for phosphates compared to oxides. This inductive effect makes several couples that are attractive in oxides, such as Mn^{3+}/Mn^{4+}, Fe^{3+}/Fe^{4+}, Cr^{3+}/Cr^{4+}, Cu^{2+}/Cu^{3+} Co^{2+}/Co^{3+}, Co^{3+}/Co^{4+}, Ni^{2+}/Ni^{3+}, and Ni^{3+}/Ni^{4+}, too high in voltage for commercial electrolytes, even though they might be of interest with advanced electrolyte technology. We should note, however, that this statement is statistical, and some of those couples, if present in the right low voltage crystal structure, could show activity at voltages lower than 4.5 V. This is especially true for couples with an average voltage very close to the 4.5 V limit such as Mn^{3+}/Mn^{4+}. Besides the inductive effect, we find that the electrostatic and the P/O ratio also influence the voltage.

In terms of safety, the common statement that olivine-based compounds and phosphates in general are intrinsically safer than oxides is challenged by our results. Thermodynamically, we compute that most phosphate compounds evolve oxygen at lower temperature than oxides for the same oxidation state of the active redox metal. Phosphates can, however, provide in most situations cathode materials with higher voltages than oxides for a similar thermal stability. Hence, the reason that $LiFePO_4$ is so stable against reduction by the electrolyte should at least in part be attributed to its low voltage. This is consistent with our computational and recent experimental evidence that indicates that the higher voltages olivine ($LiMnPO_4$, $LiCoPO_4$, and $LiNiPO_4$) do not share the excellent thermal stability of $LiFePO_4$. The inherent safety of phosphates is often extended to polyanionic systems in general (e.g., silicates[103]) and this calls for a future similar computational investigation of those alternative polyanionic chemistries.

If one generalizes to other polyanions the observation made on phosphates, high inductive effect polyanions such as sulfates, fluoro-phosphates, and fluoro-sulfates might provide the highest voltage for a given thermal stability.

On the basis of our data, the only one-electron couples presenting acceptable safety combined with voltages in the 3−4.5 V window and that are lightweight are Fe^{2+}/Fe^{3+}, Mn^{2+}/Mn^{3+}, and Cu^{1+}/Cu^{2+}. The two first couples have been extensively studied in olivine $LiMPO_4$. While iron olivine is definitely a successful cathode material, the manganese version shows much poorer electrochemical performances.[105] Our work identifies some new opportunities for these redox couples. We find that energetically competitive tetrahedral structures based on LISICON exist. These alternative structures, if they are successfully synthesized, might provide similar energy densities than the olivines. The Cu^{1+}/Cu^{2+} couple is not commonly used in Li batteries. Our analysis shows that the combination of the higher

maximal capacity for +1/+2 compounds with the acceptable average voltage around 3.2 V makes it theoretically possible to surpass the iron olivine's 600 Wh/kg specific energy limit. Unfortunately, no stable lithium-containing Cu^{1+} phosphate is known, and none was predicted to be stable in this work. The stability analysis showed a Cu^{1+} phosphate in tetrahedral coordination at composition $Li_5Cu(PO_4)_2$ in a LISICON structure as closest to the hull. This compound lies 20 meV/at above its decomposition products: Cu, Cu_2O, Li_3PO_4, and $Li_2CuP_2O_7$. The $Li_3Cu_3(PO_4)_2$ would be more interesting in terms of gravimetric capacity and is computed to be 54 meV/at above the hull in the LISICON structure. Two potential issues with a battery working on the Cu^{1+}/Cu^{2+} couple would be the very different preferred local environment for the Cu^{1+} and Cu^{2+} ions (tetrahedral and octahedral or square planar) and the high mobility of Cu^{1+}. Both effects could make it difficult to retain the crystal structure upon cycling.

Because of the limitations on the gravimetric and volumetric capacity of phosphates, two-electron systems are of strong interest with this anion chemistry. Our analysis shows that few elements could provide two-electron activity in the 3−4.5 V voltage window. No M^{2+}/M^{4+} redox couple was found to satisfy those requirements. Only molybdenum (Mo^{3+} to Mo^{6+}) and vanadium (V^{3+} to V^{5+}) show redox couples in the targeted voltage window with high enough achievable gravimetric capacities. In addition, those two elements are stable in phosphates in an octahedral environment for all oxidation states and are in general relatively thermally stable. Our compound prediction algorithm identified a novel two-electron vanadium compound, $Li_9V_3(P_2O_7)_3(PO_4)_2$, to be very close to stability at zero K (7 meV/at above the hull). This mixed ortho- and pyrophosphate, isostructural to $Li_9Fe_3(P_2O_7)_3(PO_4)_2$,[106] presents attractive theoretical specific energy (726 Wh/kg) and has been synthesized and tested electrochemically in our research group.[107] Very recently, Kuang et al. reported independently on the synthesis and electrochemical testing of this compound.[108]

The Sb^{3+}/Sb^{5+} redox couple is also of interest, but the weight of antimony combined with the strong preference for different local environment for Sb^{3+} and Sb^{5+} (8-fold coordinated and octahedral) are detrimental.

Oxyphosphates are an attractive subclass of phosphates with their possible higher capacity because of their lower phosphorus content, while still benefiting from the inductive effect. In addition, the connectivity of their transition metal octahedra might be favorable for electronic conductivity. Only a few oxyphosphates are known. Most of them exist in vanadium, molybdenum, and titanium chemistries. The lithium vanadium oxyphosphate $LiVOPO_4$ has been already well studied and shows good specific energy but poor rate capability.[75] The two-electron redox couples available for vanadium and molybdenum combined with their tendency to form oxyphosphates call for more investigations of these chemistries.

The data provided in this work can be used to propose new chemistries to explore but also to suggest incremental modifications to known compounds. For instance, the vanadium NASICON $Li_3V_2(PO_4)_3$ is a promising battery cathode with a computed theoretical energy density of 724 Wh/kg and 2099 Wh/l.[8,109] Unfortunately, the last lithium extraction process shows an important hysteresis, and only the capacity related to the V^{3+}/V^{4+} couple can be used practically. Without this last lithium, the theoretical energy density (456Wh/kg and 1330 Wh/l) is much lower than that of $LiFePO_4$. On the other hand, our calculations predict that molybdenum also forms a $Li_3Mo_2(PO_4)_3$ NASICON structure. This molybdenum compound is not very competitive by itself in terms of energy densities (526 Wh/kg and 1732Wh/l). However, by replacing one-quarter of the nonactive vanadium in $Li_3V_2(PO_4)_3$ by Mo^{3+}, it might be possible to extract this last lithium with lower hysteresis. This strategy suggests a $Li_3Mo_{0.5}V_{1.5}(PO_4)_3$ compound with a competitive theoretical specific energy of 654 Wh/kg (3.5 V average voltage with a capacity of 187 mAh/g). The energy density is also attractive at 1900 Wh/l. Both specific energy and energy density are competitive with $LiFePO_4$ (600 Wh/kg and 1900 Wh/l). In addition, computations predict that molybdenum would mix easily in the vanadium NASICON structure. The best ordering for $Li_3Mo_{0.5}V_{1.5}(PO_4)_3$ is 4 meV/at (or 40 meV/transition metal sites) above the hull and within the range where entropy effects will stabilize the mixing. This example illustrates how a high-throughput computational study can be used to help the rational design of new battery compounds.

It is remarkable that for all properties investigated, except the voltage, $LiFePO_4$ is close to the optimal of what could be expected from a one-electron phosphate. The 170 mAh/g capacity is the highest achievable (except for oxyphosphates). Olivines are among the most dense phosphate compounds with volumetric capacities around 590 mAh/cm^3, and the safety of the delithiated iron olivine is extremely good for a material working at 3.5 V. Hence, unless one can increase the voltage of olivines without sacrificing other properties, not much improvement should be expected for one-electron phosphates.

All battery properties cannot be directly computed *ab initio* on a large scale, and our investigations only focused on some necessary but not sufficient conditions that new phosphate cathodes should meet. We believe the developments in accurate modeling of lithium diffusion[110] and polaron migration[111,112] will in the future provide the ability to perform the same kind of analysis on a larger set of properties such as ionic and electronic conductivity. Beside the difficulties in accurately modeling those properties, many challenges lies in the scaling up of their computations without human intervention in a high-throughput framework.

5. CONCLUSION

We have performed a large scale computational evaluation of phosphates as cathode materials. A computational database of thousands of known and virtual phosphate materials has been built. Essential battery properties such as stability, capacity (volumetric and gravimetric), voltage, specific energy, energy density, and safety have been computed using this data. Limits and opportunities in phosphate chemistries have been evaluated. Such a high-throughput approach can help the experimental process of new cathode materials design focus on the most promising directions and will be extended in the future to other chemistries.

■ ASSOCIATED CONTENT

Supporting Information. Stability results for lithium-containing ICSD phosphates, relative stability of $LiCoPO_4$ phases with different functionals, and details on the ANOVA analysis of the factors determining the voltage. This information is available free of charge via the Internet at http://pubs.acs.org/

AUTHOR INFORMATION

Corresponding Author
*E-mail: gceder@mit.edu.

ACKNOWLEDGMENT

The authors would like to acknowledge Bosch and Umicore for funding. Anubhav Jain acknowledges funding from the U.S. Department of Energy, Department of Energy Computational Science Graduate Fellowship (DOE CSGF) (under Grant DE-FG02-97ER25308).

REFERENCES

(1) Whittingham, M. S. *Chem. Rev.* **2004**, *104*, 4271–4302.
(2) Padhi, A.; Nanjundaswamy, K.; Goodenough, J. B. *J. Electrochem. Soc.* **1997**, *144*, 1188.
(3) Masquelier, C.; Patoux, S.; Wurm, C.; Morcrette, M. In *Polyanion-Based Positive Electrode Materials*; Nazri, G.-A., Pistoia, G., Eds.; Springer: New York, 2003; pp 445−474.
(4) Whittingham, M. S.; Song, Y.; Lutta, S.; Zavalij, P. Y.; Chernova, N. A. *J. Mater. Chem.* **2005**, *15*, 3362.
(5) Delacourt, C.; Poizot, P.; Morcrette, M.; Tarascon, J.-M.; Masquelier, C. *Chem. Mater.* **2004**, *16*, 93–99.
(6) Gaubicher, J.; Mercier, T. L.; Chabre, Y.; Angenault, J.; Quarton, M. *J. Electrochem. Soc.* **1999**, *146*, 4375–4379.
(7) Patoux, S.; Wurm, C.; Morcrette, M.; Rousse, G.; Masquelier, C. *J. Power Sources* **2003**, *119−121*, 278–284.
(8) Saïdi, M.; Barker, J.; Huang, H.; Swoyer, J. L.; Adamson, G. *J. Power Sources* **2003**, *119−121*, 266–272.
(9) Ceder, G.; Chiang, Y.-M.; Sadoway, D. R.; Aydinol, M.; Jang, Y. I.; Huang, B. *Nature* **1998**, *392*, 694–696.
(10) Van Der Ven, A.; Aydinol, M. K.; Ceder, G. *J. Electrochem. Soc.* **1998**, *145*, 2149.
(11) Kang, K.; Meng, Y. S.; Bréger, J.; Grey, C. P.; Ceder, G. *Science* **2006**, *311*, 977–980.
(12) Kang, B.; Ceder, G. *Nature* **2009**, *458*, 190–193.
(13) Meng, Y. S.; Wu, Y. W.; Hwang, B. J.; Li, Y.; Ceder, G. *J. Electrochem. Soc.* **2004**, *151*, A1134.
(14) Arroyo-deDompablo, M. E.; Dominko, R.; Gallardo-Amores, J. M.; Dupont, L.; Mali, G.; Ehrenberg, H.; Jamnik, J.; Morán, E. *Chem. Mater.* **2008**, *20*, 5574–5584.
(15) Arroyo Y De Dompablo, M.; Amador, U.; Tarascon, J.-M. *J. Power Sources* **2007**, *174*, 1251–1257.
(16) Ceder, G.; Hautier, G.; Jain, A.; Ong, S. P. *MRS Bull.* **2011**, *36*, 185–191.
(17) Meng, Y. S.; Arroyo-de Dompablo, M. E. *Energy Environ. Sci.* **2009**, *2*, 589.
(18) Armstrong, a. R.; Arrouvel, C.; Gentili, V.; Parker, S. C.; Islam, M. S.; Bruce, P. G. *Chem. Mater.* **2010**, *2*, 101117124944079.
(19) Kim, J. C.; Moore, C. J.; Kang, B.; Hautier, G.; Jain, A.; Ceder, G. *J. Electrochem. Soc.* **2011**, *158*, A309.
(20) Perdew, J.; Burke, K.; Ernzerhof, M. *Phys. Rev. Lett.* **1996**, *77*, 3865–3868.
(21) Anisimov, V.; Zaanen, J.; Andersen, O. *Phys. Rev. B* **1991**, *44*, 943–954.
(22) Anisimov, V. I.; Aryasetiawan, F.; Lichtenstein, A. I. *J. Phys.: Condens. Matter* **1997**, *9*, 767–808.
(23) Kubaschewski, O.; Alcock, C. B.; Spencer, P. J. In *Thermochemical Data*, 6th ed.; Pergamon Press:Elmsford, NY, 1993; Chapter 5, pp 257−323.
(24) Wang, L.; Maxisch, T.; Ceder, G. *Phys. Rev. B* **2006**, *73*, 1–6.
(25) Zhou, F.; Cococcioni, M.; Kang, K.; Ceder, G. *Electrochem. Commun.* **2004**, *6*, 1144–1148.
(26) Heyd, J.; Scuseria, G. E.; Ernzerhof, M. *J. Chem. Phys.* **2003**, *118*, 8207.
(27) Chevrier, V. L.; Ong, S. P.; Armiento, R.; Chan, M. K. Y.; Ceder, G. *Phys. Rev. B* **2010**, *82*, 075122.
(28) Kresse, G.; Furthmuller, J. *Comput. Mater. Sci.* **1996**, *6*, 15–50.
(29) Blöchl, P. *Phys. Rev. B* **1994**, *50*, 17953–17979.
(30) Jain, A.; Hautier, G.; Moore, C. J.; Ong, S. P.; Fischer, C. C.; Mueller, T.; Persson, K. A.; Ceder, G. *Comput. Mater. Sci.* **2011**, *50*, 2295–2310.
(31) *Inorganic Crystal Structure Database*; FIZ Karlsruhe: Germany, 2006.
(32) Burzlaff, H.; Malinovsky, Y. *Acta Crystallogr., Sect. A: Found. Crystallogr.* **1997**, *53*, 217–224.
(33) Hundt, R.; Schön, J. C.; Jansen, M. *J. Appl. Crystallogr.* **2006**, *39*, 6–16.
(34) Hart, G. L. W.; Forcade, R. W. *Phys. Rev. B* **2008**, *77*, 1–12.
(35) Hautier, G.; Fischer, C.; Ehrlacher, V.; Jain, A.; Ceder, G. *Inorg. Chem.* **2011**, *50*, 656–663.
(36) Ong, S. P.; Wang, L.; Kang, B.; Ceder, G. *Chem. Mater.* **2008**, *20*, 1798–1807.
(37) Hautier, G.; Fischer, C. C.; Jain, A.; Mueller, T.; Ceder, G. *Chem. Mater.* **2010**, *22*, 3762–3767.
(38) O'Keefe, M. *Acta Crystallogr., Sect. A* **1979**, *35*, 772–775.
(39) Pinsky, M.; Avnir, D. *Inorg. Chem.* **1998**, *37*, 5575–5582.
(40) Aydinol, M.; Kohan, A.; Ceder, G.; Cho, K.; Joannopoulos, J. *Phys. Rev. B* **1997**, *56*, 1354–1365.
(41) Jain, A.; Hautier, G.; Ong, S. P.; Moore, C. J.; Fischer C. C.; Persson, K. A.; Ceder, G. *Phys. Rev. B* **2011**, accepted.
(42) Ong, S. P.; Jain, A.; Hautier, G.; Kang, B.; Ceder, G. *Electrochem. Commun.* **2010**, *4*, 1–4.
(43) Chase, M. W. *NIST-JANAF Thermochemical Tables*; American Institute of Physics: Woodbury, NY, 1998.
(44) Durif, A. *Crystal Chemistry of Condensed Phosphates*; Plenum Press, New York, 1995.
(45) Yin, S.-C.; Grondey, H.; Strobel, P.; Anne, M.; Nazar, L. F. *J. Am. Chem. Soc.* **2003**, *125*, 10402–11.
(46) Laügt, M.; Tordjman, I.; Guitel, J. C.; Roudaut, R. *Acta Crystallogr., Sect. B: Struct. Crystallogr. Cryst. Chem.* **1972**, *28*, 2352–2358.
(47) Laügt, M.; Durif, A.; Martin, C. *J. Solid State Chem.* **1974**, *7*, 448.
(48) García-Moreno, O.; Alvarez-Vega, M.; García-Alvarado, F.; García-Jaca, J.; Gallardo-Amores, J. M.; Sanjuán, M. L.; Amador, U. *Chem. Mater.* **2001**, *13*, 2455–2455.
(49) Averbuch-Pouchot, M. T. *Acta Crystallogr., Sect. C: Cryst. Struct. Commun.* **1989**, *45*, 1856–1858.
(50) Ramana, C. V.; Ait-Salah, A.; Utsunomiya, S.; Mauger, A.; Gendron, F.; Julien, C. M. *Chem. Mater.* **2007**, *19*, 5319–5324.
(51) Ramana, C. V.; Kopec, M.; Mauger, A.; Gendron, F.; Julien, C. M. *J. Appl. Phys.* **2009**, *106*, 064304.
(52) Murashova, E. V.; Chudinova, N. N. *Inorg. Mater.* **2000**, *36*, 1277–1281.
(53) Lesnyak, V. V.; Slobodyanik, N. S. *Theor. Exp. Chem.* **1999**, *35*, 338–342.
(54) Patoux, S.; Rousse, G.; Leriche, J.; Masquelier, C. *Solid State Sci.* **2004**, *6*, 1113–1120.
(55) Nishimura, S.-i.; Nakamura, M.; Natsui, R.; Yamada, A. *J. Am. Chem. Soc.* **2010**, *132*, 13596–7.
(56) Zhou, H.; Upreti, S.; Chernova, N. A.; Hautier, G.; Ceder, G.; Whittingham, M. S. *Chem. Mater.* **2011**, *23*, 293–300.
(57) Amador, U.; Gallardo-Amores, J.; Heymann, G.; Huppertz, H.; Morán, E.; Arroyo Y De Dompablo, M. *Solid State Sci.* **2009**, *11*, 343–348.
(58) Huang, X.; Ma, J.; Wu, P.; Hu, Y.; Dai, J.; Zhu, Z. *Mater. Lett.* **2005**, *59*, 578–582.
(59) Chippindale, A. M.; Cowley, A. R.; Chen, J.; Gao, Q.; Xu, R. *Acta Crystallogr., Sect. C: Cryst. Struct. Commun.* **1999**, *55*, 845–847.
(60) Padhi, A.; Manivannan, V.; Goodenough, J. B. *J. Electrochem. Soc.* **1998**, *145*, 1518.
(61) Padhi, A.; Nanjundaswamy, K.; Masquelier, C.; Okada, S.; Goodenough, J. B. *J. Electrochem. Soc.* **1997**, *144*, 1609–1613.
(62) Patoux, S.; Masquelier, C. *Chem. Mater.* **2002**, *14*, 5057–5068.

(63) Yang, Z.; Choi, D.; Kerisit, S.; Rosso, K. M.; Wang, D.; Zhang, J.; Graff, G.; Liu, J. *J. Power Sources* **2009**, *192*, 588–598.
(64) Kuhn, A.; Martín, M.; Garcia-Alvarado, F. *J. Solid State Chem.* **2010**, *183*, 20–26.
(65) Arroyo-de Dompablo, M. E.; Gallardo-Amores, J. M.; Amador, U. *Electrochem. Solid-State Lett.* **2005**, *8*, A564.
(66) Ait-Salah, A.; Ramana, C. V.; Gendron, F.; Morhange, J.; Mauger, A.; Selmane, M.; Julien, C. M. *Mater. Res. Soc. Symp. Proc.* **2007**, *972*.
(67) Delmas, C.; Nadiri, A.; Soubeyroux, J. L. *Solid State Ionics* **1988**, 419–423.
(68) Aatiq, A.; Menetrier, M.; Croguennec, L.; Suard, E.; Delmas, C. *J. Mater. Chem.* **2002**, *12*, 2971–2978.
(69) Kishore, M.; Pralong, V.; Caignaert, V.; Varadaraju, U.; Raveau, B. *J. Power Sources* **2007**, *169*, 355–360.
(70) Bhuvaneswari, G. D.; Kalaiselvi, N. *Appl. Phys. A: Mater. Sci. Process.* **2009**, *96*, 489–493.
(71) Gaubicher, J.; Wurm, C.; Goward, G.; Masquelier, C.; Nazar, L. *Chem. Mater.* **2000**, *12*, 3240–3242.
(72) Satya Kishore, M.; Pralong, V.; Caignaert, V.; Malo, S. Hebert, S.; Varadaraju, U.; Raveau, B. *J. Solid State Chem.* **2008**, *181*, 976–982.
(73) Nanjundaswamy, K.; Padhi, A.; Goodenough, J. B.; Okada, S.; Otsuka, H.; Arai, H.; Yamaki, J. *Solid State Ionics* **1996**, *92*, 1–10.
(74) Dupré, N.; Gaubicher, J.; Le Mercier, T.; Wallez, G.; Angenault, J.; Quarton, M. *Solid State Ionics* **2001**, *140*, 209–221.
(75) Barker, J.; Saidi, M. Y.; Swoyer, J. L. *J. Electrochem. Soc.* **2004**, *151*, A796.
(76) Kerr, T. A.; Gaubicher, J.; Nazar, L. F. *Electrochem. Solid-State Lett.* **2000**, *3*, 460–462.
(77) Kishore, M. S.; Pralong, V.; Caignaert, V.; Varadaraju, U.; Raveau, B. *Solid State Sci.* **2008**, *10*, 1285–1291.
(78) Wolfenstine, J.; Allen, J. *J. Power Sources* **2005**, *142*, 389–390.
(79) Wolfenstine, J.; Allen, J. *J. Power Sources* **2004**, *136*, 150–153.
(80) Amine, K. *Electrochem. Solid-State Lett.* **1999**, *3*, 178.
(81) Wohlfahrt-Mehrens, M. Lithium Ion Batteries: Battery Materials and Ageing Processes. Conference on Advanced Battery Technologies for Automobiles and Their Electric Power Grid Integration, 2010.
(82) Choi, S.; Hong, S.-T. *Mater. Res. Bull.* **2005**, *40*, 1787–1795.
(83) Uebou, Y. *Solid State Ionics* **2002**, *148*, 323–328.
(84) Uebou, Y.; Okada, S.; Yamaki, J.-i. *J. Power Sources* **2003**, *115*, 119–124.
(85) Sahai, H.; Ageel, M. I. *Analysis of Variance: Fixed, Random and Mixed Models*; Birkhäuser: Boston, 2000; p 784.
(86) Arroyo-de Dompablo, M.; Armand, M.; Tarascon, J.; Amador, U. *Electrochem. Commun.* **2006**, *8*, 1292–1298.
(87) Howard, W.; Spotnitz, R. *J. Power Sources* **2007**, *165*, 887–891.
(88) Dahn, J.; Fuller, E.; Obrovac, M.; Vonsacken, U. *Solid State Ionics* **1994**, *69*, 265–270.
(89) Xu, K. *Chem. Rev.* **2004**, *104*, 4303–4418.
(90) MacNeil, D. D.; Zhonghua, L.; Zhaohui, C.; Dahn, J. R. *J. Power Sources* **2002**, *108*, 8–14.
(91) Godshall, N. A.; Raistrick, I. D.; Huggins, R. A. *J. Electrochem. Soc.* **1984**, *131*, 543.
(92) Huggins, R. A. *ECS Trans.* **2009**, *16*, 37–47.
(93) Delacourt, C.; Poizot, P.; Tarascon, J.-M.; Masquelier, C. *Nat. Mater.* **2005**, *4*, 254–260.
(94) Kim, S.-W.; Kim, J.; Gwon, H.; Kang, K. *J. Electrochem. Soc.* **2009**, *156*, A635.
(95) Chen, G.; Richardson, T. J. *J. Power Sources* **2010**, *195*, 1221–1224.
(96) Bramnik, N. N.; Nikolowski, K.; Trots, D. M.; Ehrenberg, H. *Electrochem. Solid-State Lett.* **2008**, *11*, A89.
(97) Okada, S.; Ueno, M.; Uebou, Y.; Yamaki, J. *J. Power Sources* **2005**, *146*, 565–569.
(98) Wang, D.; Xiao, J.; Zu, W.; Zhang, J.-G. Investigation of $LiNiPO_4$ as a Cathode Material for Lithium Ion Battery; International Meeting on Lithium Batteries, 2010.
(99) Huang, H.; Faulkner, T.; Barker, J.; Saidi, M. *J. Power Sources* **2009**, *189*, 748–751.
(100) Yamada, A.; Kudo, Y.; Liu, K.-Y. *J. Electrochem. Soc.* **2001**, *148*, A747.
(101) Shanmukaraj, D.; Murugan, R. *Ionics* **2004**, *10*, 88–92.
(102) Lyness, C.; Delobel, B.; Armstrong, A. R.; Bruce, P. G. *Chem. Commun.* **2007**, 4890.
(103) Nyten, A.; Abouimrane, A.; Armand, M.; Gustafsson, T.; Thomas, J. *Electrochem. Commun.* **2005**, *7*, 156–160.
(104) Jouanneau, S.; MacNeil, D. D.; Lu, Z.; Beattie, S. D.; Murphy, G.; Dahn, J. R. *J. Electrochem. Soc.* **2003**, *150*, A1299.
(105) Kang, B.; Ceder, G. *J. Electrochem. Soc.* **2010**, *157*, A808.
(106) Poisson, S.; D'Yvoire, F.; Nguyen Huy, D.; Bretey, E.; Berthet, P. *J. Solid State Chem.* **1998**, *138*, 32–40.
(107) Ceder, G.; Jain, A.; Hautier, G.; Kim, J. C.; Kang, B.; Daniel, R. *Mixed Phosphate-Diphosphate Electrode Materials and Methods of Manufacturing Same*. Patent PCT application PCT/US11/031946, 2011.
(108) Kuang, Q.; Xu, J.; Zhao, Y.; Chen, X.; Chen, L. *Electrochim. Acta* **2011**, *56*, 2201–2205.
(109) Barker, J.; Huang, H.; Swoyer, J. L.; Adamson, G. *Electrochem. Solid-State Lett.* **2002**, *5*, A149–A151.
(110) Kang, K.; Morgan, D.; Ceder, G. *Phys. Rev. B* **2009**, *79*, 1–4.
(111) Maxisch, T.; Zhou, F.; Ceder, G. *Phys. Rev. B* **2006**, *73*, 1–6.
(112) Ong, S.; Chevrier, V.; Ceder, G. *Phys. Rev. B* **2011**, *83*, 1–7.